Insect Biochemistry and Molecular Biology 43 (2013) 572–579

Contents lists available at SciVerse ScienceDirect

Insect Biochemistry and Molecular Biology

journal homepage: www.elsevier.com/locate/ibmb

Silverfish silk is formed by entanglement of randomly coiled protein chains

Andrew A. Walker [a,b], Jeffrey S. Church [c], Andrea L. Woodhead [c], Tara D. Sutherland [b,*]

[a] Research School of Biology, Australian National University, Canberra, ACT 0200, Australia
[b] CSIRO Ecosystem Sciences, Canberra 2601, Australia
[c] CSIRO Materials Science and Engineering, Waurn Ponds, Victoria 3216, Australia

ARTICLE INFO

Article history:
Received 22 November 2012
Received in revised form
25 March 2013
Accepted 26 March 2013

Keywords:
Raman spectroscopy
FTIR
Random coil
Ctenolepisma
Apterygote

ABSTRACT

Silks are semi-crystalline solids in which protein chains are associated by intermolecular hydrogen bonding within ordered crystallites, and by entanglement within unordered regions. By varying the type of protein secondary structure within crystallites and the overall degree of molecular order within fibers, arthropods produce fibers with a variety of physical properties suited to many purposes. We characterized silk produced as a tactile stimulus during mating by the grey silverfish (*Ctenolepisma longicaudata*) using Fourier transform infrared spectroscopy, polarized Raman spectroscopy, gel electrophoresis and amino acid analysis. Fibers were proteinaceous—the main component being a 220 kDa protein—and were rich in Gln/Glu, Leu, and Lys. The protein structure present was predominantly random coil, with a lesser amount of beta-structure. Silk fibers could readily be solubilized in aqueous solutions of a mild chaotrope, sodium dodecyl sulfate, indicating protein chains were not cross-linked by disulfide or other covalent bonds. We conclude that entanglement is the major mechanism by which these silk proteins cohere into a solid material. We propose silks used as short-term tactile cues are subject to less stringent requirements for molecular order relative to other silks, allowing the random coil structure to be favored as an adaptation promoting maximal entanglement and adhesion.

1. Introduction

The best-understood silks are those of silkworms and spiders, which are semi-crystalline solids containing ordered crystallites of beta-sheets embedded in regions of unordered protein chains (Fu et al., 2009; Porter and Vollrath, 2009). In these model silks, protein chains cohere to form a solid material due to extensive intermolecular hydrogen bonding within the beta-sheet crystallites and entanglement within unordered portions of the protein chains. Since crystallites and unordered regions have distinct deformational properties, they lend different mechanical properties to the material: ordered crystallites confer tensile strength (Krasnov et al., 2008) and resistance to proteolysis (Arai et al., 2004), while unordered protein regions confer flexibility (Krasnov et al., 2008) and allow entanglement (Fu et al., 2009).

Many arthropod groups besides silkworms and spiders have independently evolved the ability to produce silk (Sutherland et al., 2010). Arthropod silks are structurally diverse at the molecular level, containing crystallites of a) beta-sheets with the protein backbone parallel to the fiber axis (IIß; akin to silkworm or spider silks), b) beta-sheets with the backbone perpendicular to the fiber axis (Xβ; Weisman et al., 2009), c) alpha-helices as coiled coils (Sutherland et al., 2011), d) collagen triple helices (Rudall, 1962), or e) polyglycine II-like structures (Rudall, 1962). The ordered protein structures in silk are understood to contribute extensively to silk function—for example, Xβ crystallites confer extensibility to fibers due to their capacity for deformation-induced transitions into the IIß structure (Hepburn et al., 1979; Rudall, 1962). In contrast, the physiological, molecular and evolutionary constraints that determine the proportion of disordered protein in silk fibers is not well understood.

A necessary development for the evolution of terrestrial insects from aquatic crustaceans (Shultz and Regier, 2000) was a method of transferring sperm on dry land. Unlike pterygote insects, which developed copulation, most silverfish (order Thysanura) and bristletails (order Archaeognatha) transfer sperm with the assistance of silk produced from dermal glands on the phallus (or associated structures) of males (Bitsch, 1990; Sturm and Machida, 2001). Deposition of sperm droplets or spermatophores on silk fibers or

* Corresponding author. Building 101, Black Mountain Laboratories, Clunies, Ross Dr, Acton, ACT 2601, Australia. Tel.: +61 2 6246 4236; fax: +61 2 6246 4000.
E-mail address: Tara.Sutherland@csiro.au (T.D. Sutherland).

0965-1748/$ – see front matter
http://dx.doi.org/10.1016/j.ibmb.2013.03.014

stalks is practiced by bristletails (Sturm and Machida, 2001), the 'relic' silverfish *Tricholepidion gertschi* (Sturm, 1997), and some of the more familiar domestic silverfish (family Lepismatidae; Sturm, 1987). Lepismatids such as the European silverfish (*Lepisma saccharina*) are exceptions, as they deposit enclosed spermatophores directly onto surfaces in their environment. Perhaps surprisingly, *L. saccharina* has retained silk production as part of a highly choreographed courtship behavior (Sturm, 1956). Approaching the end of the courtship ritual, which consists of antenna-tapping and repeated responsive movements between male and female (Sturm, 1956,1987), male *L. saccharina* cover an area of the substrate with Y-shaped networks of fibers and deposit a spermatophore nearby. Detection of the Y-shaped tactile cues by the female induces a sequence of behaviors that culminates in her uptake of the spermatophore (Sturm, 1956).

The primary use of silk as a tactile cue is unusual among insects. Whilst the caterpillar *Yponomeuta cagnagellus* does use silk as a tactile cue associated with trail-following behavior, the primary use of the silk is as a cocoon material (Roessingh, 1989). To our knowledge, nothing is known about the composition or molecular biology of silverfish silk, or how its molecular structure relates to its unusual function. In this study we present results obtained from silk fibers of the lepismatid silverfish *Ctenolepisma longicaudata* (Fig. 1), a species native to South Africa which is now common in human habitations in south-eastern Australia (Watson and Li, 1967). Using Fourier transform infrared spectroscopy, Raman spectroscopy, gel electrophoresis and amino acid analysis, we investigated the silk's molecular structure and composition. We show silverfish silk to consist of large, disordered proteins, and discuss the results in relation to silk fabrication and molecular structure.

2. Results

2.1. Silverfish produce very fine non-birefringent silken threads

Silverfish (*Ctenolepisma longicaudata*) were collected from human habitations in Canberra, Australia, and housed with plastic card 'leaf-litter' over a six-month period. Inspection of plastic cards in the enclosure revealed spermatophores deposited directly on the substrate, together with deposits of silk and shed scales. Electron microscopy revealed silk filaments to be very fine, between 0.3 and 1 μm in diameter (Fig. 2). Deposits of silk consisted of bundles and cross-hatched 'grids'. These features are similar to those previously reported for the closely related silverfish *Lepisma saccharina* (Sturm, 1956) suggesting *C. longicaudata* silk is used as a tactile cue during courtship in a similar way to *L. saccharina* silk.

Fig. 1. The grey silverfish, *Ctenolepisma longicaudata*. This adult male is resting on textured plastic card.

Silk fibers could be manually drawn from the phallic glands of immobilized males by brushing the silk glands with a toothpick or pipette tip, and wound using a motorized spindle (Fig. 2D). Freshly produced silk fibers were flexible and sticky, becoming brittle after drying. Birefringence—a property of anisotropic materials evident when materials are placed between crossed polarizing filters—was low or absent in naturally produced and manually harvested silk, suggesting molecular orientation to be poor or absent.

2.2. Silverfish silk has low chemical stability and is made from high molecular weight proteins

To investigate their chemical stability, manually drawn silverfish silk fibers were immersed in chaotrope solutions at room temperature including saturated (9 M) lithium bromide, 6 M guanidinium hydrochloride, or 3% sodium dodecyl sulfate (SDS). Silk fibers dissolved readily in each chaotrope solution, with fibers immersed in 3% SDS at 25 °C dissolving completely within half an hour. The dissolution of fibers at room temperature and without the addition of reducing agents indicated a) a low chemical stability in comparison to other silks, and b) silk proteins were not covalently cross-linked into a continuous network.

Silk fibers from individual males were solubilized in 3% SDS and analyzed by polyacrylamide gel electrophoresis (PAGE). In samples from all individuals, the main protein component resolved as a sharp band with molecular weight in excess of 220 kDa (Fig. 3). More weakly staining bands with molecular weights between 60 and 70 kDa were also observed. The migration pattern of the dominant protein bands on SDS-polyacrylamide gels was consistent between individuals. Minor differences in the migration pattern of the low molecular weight proteins were observed, possibly due to allelic differences between individuals.

2.3. Silverfish silk consists of randomly coiled proteins

To examine the molecular structure and amino acid composition of silverfish silk, we obtained Fourier transform infrared (FTIR) and micro-Raman spectra from silk samples manually drawn from the glands of males.

The infrared spectrum (Fig. 4) shows maxima in the amide I region at 1651 cm^{-1}, in the amide II region at 1540 cm^{-1}, and in the amide III region at 1242 cm^{-1}. The results of second derivative spectroscopy and deconvolution analysis of the amide I and III regions, used to estimate the proportion of each secondary structure in the silk, is summarized in Table 1. Second derivative plots suggested the presence of eight bands in the amide I region (Fig. S1) and three bands in the amide III region (Fig. S2). Spectral deconvolutions (Figs. S3 and S4) suggest the silk to be rich in random coils (35–52%) and beta-sheets (43–58%) with a low content of alpha-helices (6–7%).

The silk was further examined by micro-Raman spectroscopy, which yields information about protein orientation and the content of specific amino acids in addition to conformational data. The Raman spectrum of manually drawn silk, obtained with the laser polarization parallel to the fiber axis, is shown in Fig. 5. The position of the amide I maximum at 1664 cm^{-1} was consistent with random coil or beta-sheet protein conformations or a mixture both conformations (Fabian and Anzenbacher, 1993; Frushour and Koenig, 1975; Rousseau et al., 2004); the amide III maximum at 1243 cm^{-1} favors random coil structure (Fabian and Anzenbacher, 1993; Frushour and Koenig, 1975; Rousseau et al., 2004). Disorder in protein chains was further indicated by the tyrosine (Tyr) peak. The 850 cm^{-1} component of the Fermi doublet dominates the

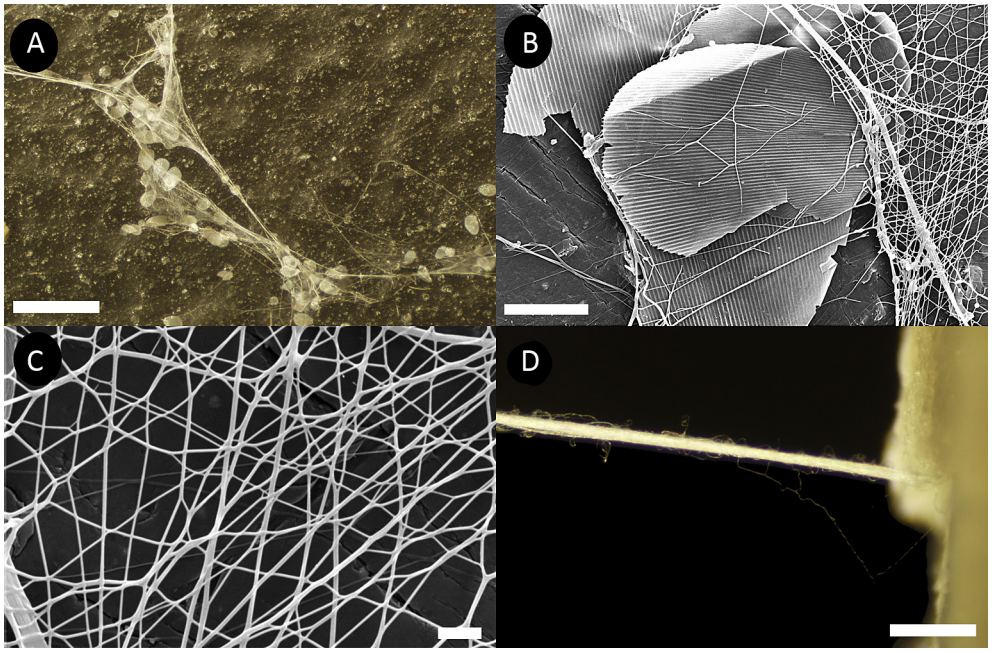

Fig. 2. Silverfish silk. A, silk deposit on plastic card from housing chamber, with shed scales; scale bar is 200 μm. B, scanning electron micrograph showing silverfish scales and silk; scale bar is 20 μm. C, scanning electron micrograph showing sub-micrometer threads cross-hatched to form a grid; scale bar is 5 μm. D, bundle of manually collected silk fibers; scale bar is 200 μm.

830 cm^{-1} component, suggesting hydroxyl groups of Tyr residues are rarely hydrogen bonded to other amino acids (Siamwiza et al., 1975).

Results of the second derivative and deconvolution analysis performed on Raman amide I and amide III regions are shown in Table 2. The second derivative plot of the Raman spectrum amide I region (Fig. S5) suggested the presence of 5 conformational component bands, though several were at the noise level of the second derivative spectrum. In the spectral deconvolution of the amide I region based on the identified band components (Fig. S6), the 1640 cm^{-1} band assigned to random coil comprises 28% of the band envelope. This is consistent with the assignments presented by Lefèvre and et al. (2012) with the argument that the low symmetry of the silk protein has caused this normally Raman inactive mode to be observed. It is likely an additional random coil component is present in the 1659 to 1669 cm^{-1} region of the second derivative plot (Fig. S5) but is being masked by the intense, broad feature at 1657 cm^{-1} assigned to the alpha-helical conformation. This could cause both the beta-sheet and alpha-helical content to be over-predicted in the deconvolution analysis of the amide I region. The lack of reliable fine structure on the amide I band contour makes it difficult to obtain reliable structural information from its analysis.

To better resolve the structure of the major components, protein conformation was investigated through analysis of the simpler amide III profile (Table 2). Three conformational components are evident in the plot of the second derivative (Fig. S7). The

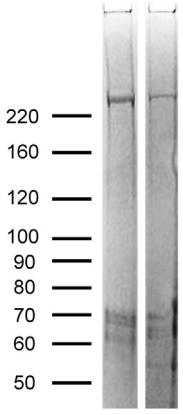

Fig. 3. SDS-PAGE of silverfish silk proteins. The two lanes correspond to silk preparations from two different males. Molecular weight markers (kDa) are shown on the left.

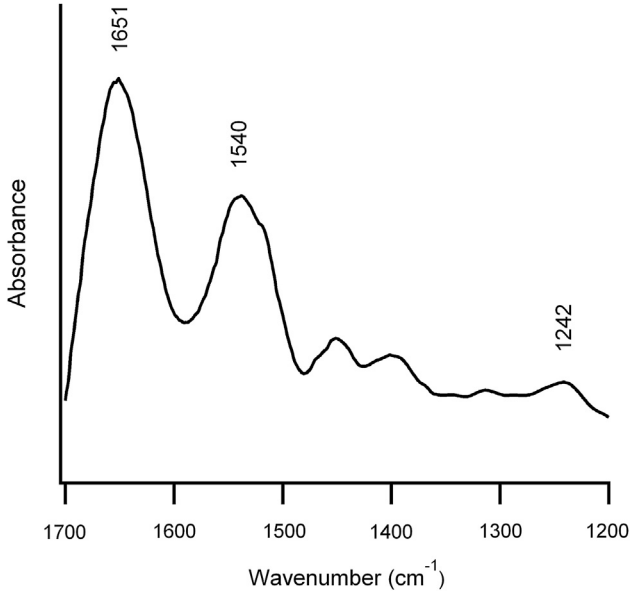

Fig. 4. FTIR spectrum of silverfish silk showing amide functional maxima at 1652, 1540, and 1241 cm^{-1}.

Table 1
Amide I and III infrared band components as identified by 2nd derivative spectroscopy and spectral deconvolution.

2nd derivative minimum (cm^{-1})	Deconvolution (cm^{-1})	Component area (%)	Assignments (Byler and Susi, 1986;Singh et al., 1993.)
Amide I			
1692	1693	3	Beta-sheet
1682	1683	11	Random coil
1674	1667	0	Random coil
1667	1666	30	Random coil
1659	1655	6	Alpha-helix
1651	1651	10	Random coil
1640	1641	14	Beta-sheet
1629	1625	26	Beta-sheet
Amide III			
1288	1285	7	Alpha-helix
1261	1263	35	Random coil
1238	1238	58	Beta-sheet

Table 2
Amide I and III Raman band components as identified by 2nd derivative spectroscopy and spectral deconvolution.

2nd derivative minimum (cm^{-1})	Deconvolution (cm^{-1})	Component area (%)	Assignments (Lefèvre et al., 2012)
Amide I[a]			
1690	1693	6	Beta-turn
1678	1677	25	Beta-turn
1672	1671	26	Beta-sheet[a]
1657	1655	14	Alpha-helix[a]
1641	1640	28	Random coil
Amide III			
1269	1270	9	Alpha-helix
1244	1243	91	Random coil
1227	1222	<1	Beta-sheet

[a] It is likely that random coil is significantly higher in the material than indicated in the amide I region due to the masking of this component by the intense, broad feature at 1657 cm^{-1} (see Fig. S5). Masking of the component would lead to over prediction of the beta-sheet and alpha-helical content (as described in the text).

deconvolution based on these features (Fig. 6 A) suggests a dominant random coil structure, with 9% alpha-helical content. The beta-sheet feature identified at 1227 cm^{-1} in the second derivative plot iterates to a value less than 1% (not shown).

For comparison, deconvolutions were also conducted on the amide III regions of silkworm cocoon silk and wool—materials known to consist predominantly of proteins with beta-sheet and alpha-helical conformations, respectively—using starting component peaks identified by second derivative spectra (Fig. 6B and C). The amide III region of the silkworm silk spectrum (Fig. 6B) could be resolved into a major component at 1232 cm^{-1} (beta-sheet) and minor components at 1243 cm^{-1} (random coil) and 1266 cm^{-1} (alpha-helix). The amide III region of the spectrum obtained from wool (Fig. 6C) consisted of a major component at 1271 cm^{-1} (alpha-helix) and minor components at 1245 and 1228 cm^{-1} assigned respectively to random coil and beta-sheet (Carter et al., 1994). These results are consistent with the known protein structures of these materials, and support the assignments of the amide III components observed in the silverfish silk spectrum indicating the predominant structure to be random coil.

To examine the orientation of proteins in the silk, polarized Raman spectra in the amide I region were obtained from single silverfish silk fibers naturally spun and collected from the housing chamber. Typical parallel and perpendicular spectra are shown as Fig. 7. Over the three spots analyzed, the perpendicular polarized band (maximum at 1669 cm^{-1}) was consistently found to be much sharper and 15–25% more intense than the parallel polarized band (maximum at 1664 cm^{-1}). Due to the modest signal to noise ratios

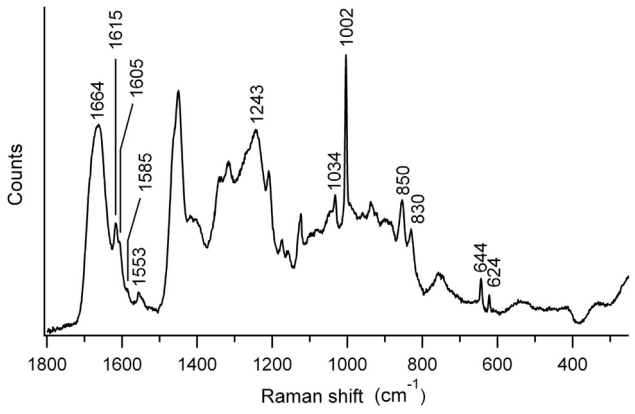

Fig. 5. Raman spectrum of silverfish silk.

in these spectra, second derivative spectroscopy was not possible and thus spectral deconvolution was not carried out. However, it is clear there is a significant protein component in which carbonyl groups are orientated perpendicular to the fiber axis. The 1669 cm^{-1} peak frequency and low level of alpha-helix present indicates the orientated protein components are beta-sheets with the peptide backbone parallel to the fiber axis—i.e. the extended-beta-sheet (IIß) structure.

In summary, the results of the infrared and Raman spectroscopy obtained from silverfish silk indicate a dominant random coil structure with moderate to comparable levels of IIß structure, and a low level of alpha-helices.

2.4. Amino acid composition of silverfish silk

The amino acid analysis of acid hydrolyzed, manually drawn silk (Table 3) revealed high proportions of Gln/Glu (14.5%), Leu (11.2%), Lys (10.9%) and Asn/Asp (10.0%). Significant proportions of the aromatic amino acids Phe (4.7%) and Tyr (3.9%) were also detected, and Met was nearly absent (0.7%). Overall, polar and charged residues made up the majority of residues recovered (57.4%) and aromatic residues were also well-represented (11.7%). The small amino acids Ala, Gly and Ser, which account for 50–80% of residues in silk made by silkworms and many other species (Lucas and Rudall, 1968), accounted for only 16.3% of the residues recovered.

The amino acid composition of silverfish silk was also investigated using Raman spectroscopy. Raman spectroscopy is able to detect amino acids such as Trp and Cys, which are destroyed by acid hydrolysis. In agreement with the direct amino acid analysis, Raman analysis (Fig. 5) found the silk to contain significant levels of aromatic amino acids: a moderately intense band observed at 1615 cm^{-1} is associated with the ring modes of the aromatic amino acids Phe, Tyr and Trp while the well resolved but weak shoulder at 1605 cm^{-1} was assigned to Phe and Tyr (Maiti et al., 2004). The very weak shoulder at 1585 cm^{-1} was assigned to Phe and Trp (Frushour and Koenig, 1975), and the feature at 1553 cm^{-1} to Trp (Frushour and Koenig, 1975). Tryptophan is destroyed during acid hydrolysis and was thus not detected by the direct amino acid analysis method. The relative weakness of the 1553 cm^{-1} feature coupled with the lack of a high wavenumber shoulder on the 1002 cm^{-1} band suggests that the concentration of Trp in the silk is low (Church et al., 1997). Phe and Tyr appear to be present in greater abundance: the strong sharp peak at 1002 cm^{-1} and the features at 1034 cm^{-1} (moderate) and 624 cm^{-1} (weak) are associated with Phe, while the 850, 830 and 644 cm^{-1} peaks are attributed to Tyr (Church et al., 1997; Frushour and Koenig, 1975). As described

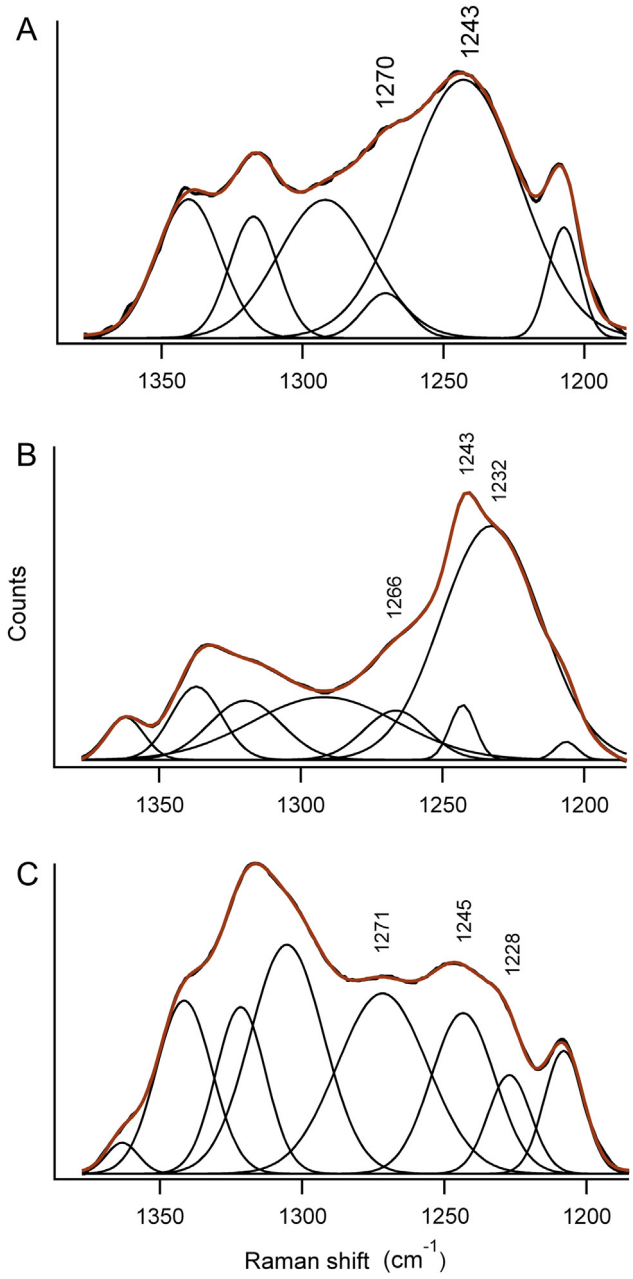

Fig. 6. Deconvolution of the amide III region of Raman spectra obtained from silverfish silk (A), silkworm (muga) cocoon silk (B) and merino wool (C). The laser polarization was parallel to the fiber axis is all cases and the red traces represent the sums of the component peaks. (For interpretation of the references to color in this figure legend, the reader is referred to the web version of this article.)

earlier, the dominant intensity of the 850 cm^{-1} component of the 850 and 830 cm^{-1} Fermi doublet suggests that the hydroxyl groups of Tyr residues are not strong hydrogen bond donors to other amino acids (Siamwiza et al., 1975), consistent with a high degree of disorder in the protein chains. The absence of any features near 650 and 700 cm^{-1} attributable to C-S stretching vibrations (Nogami et al., 1975) is consistent with the low level of methionine detected by amino acid analysis.

The direct amino acid analysis conducted did not provide information about cysteine. In the Raman spectra there was no significant feature in the region characteristic of disulfide linkages near 500 cm^{-1} (Sugeta et al., 1972; Van Wart and Scheraga, 1986)

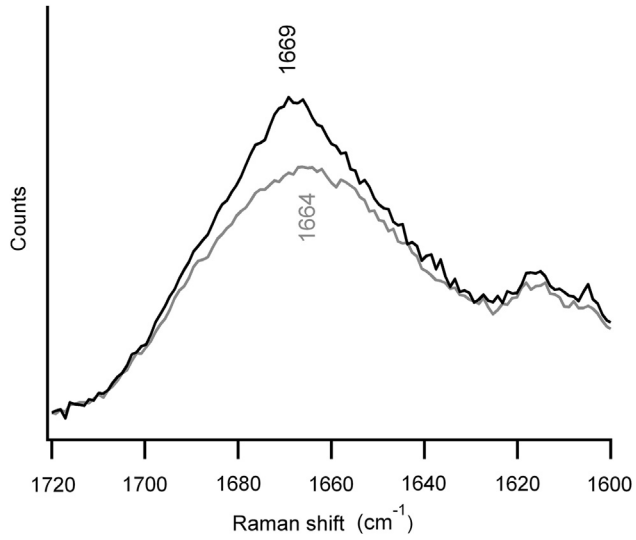

Fig. 7. Amide I region of Raman spectra obtained from silverfish silk with laser polarization perpendicular (black) or parallel (grey).

suggesting disulfide cross-linking of Cys residues occurs at low levels or is absent in silverfish silk, consistent with the observation that reducing agents were not required to solubilize the silk fibers.

3. Discussion

In this study we characterized silk produced by male grey silverfish (*Ctenolepisma longicaudata*). Silverfish silk has an unusual function in that it is used as a tactile cue during courtship (Sturm, 1956). The role of other silks used as tactile cues, such as some lepidopteran silks (Roessingh, 1989), is secondary to the main role of the silk as a cocoon material. To our knowledge, the production of silk primarily for use as a tactile cue is limited among the insects to silverfish such as *C. longicaudata* and *L. saccharina*.

Silverfish produce silk in epidermal glands (Bitsch, 1990) which are similar to the silk glands of web-spinners (Alberti and Storch, 1976; Nagashima et al., 1991) and sphecid wasps (Serrao, 2005). Silk proteins in solution are drawn through a ductule, emerging externally as solid fibers. In macroscopic appearance, silverfish fibers are typical of many insect silks—for example, we were able to draw continuous thin cylindrical fibers, up to 20 cm long and

Table 3
Amino acid composition of silverfish silk.

Amino acid	% of recovered
Ala	8.4
Cys	nd
Asp + Asn	10.0
Glu + Gln	14.5
Phe	4.9
Gly	3.1
His	3.1
Ile	2.5
Lys	10.9
Leu	11.2
Met	0.7
Pro	5.2
Arg	4.4
Ser	4.8
Thr	6.0
Val	6.5
Trp	nd
Tyr	3.7

nd = not determined.

<1 μm in diameter, directly from the glands using a motorized spool (see Section 2.1). However, the silk was found to have an unusual suite of molecular properties in comparison to previously described silks: low molecular orientation (Sections 2.1 and 2.3), low aqueous stability (Section 2.2), atypical amino acid composition (Section 2.4), and predominant random coil molecular structure (Section 2.3). Furthermore, we found no evidence of covalent cross-linking in the silk. To our knowledge, all previously described silk fibers are stabilized by cross-links in the form of either extensive hydrogen bonding within ordered crystallites (Fu et al., 2009), disulfide (Case et al., 1997) or other covalent bonds (Sutherland et al., 2006), strong electrostatic interactions such as formation of phosphoserine/metal ion complexes (Ashton et al., 2012), or some combination of these mechanisms. For silverfish silk, the high proportion of random coil structure (Section 2.3), low level of molecular orientation (Section 2.1), solubility properties (Section 2.2), and low level of tyrosine amino acid interactions all suggest the density of intermolecular hydrogen bonding to be significantly lower than found in previously characterized silks.

The absence of evidence for chemical cross-links, coupled with the large size of the silk proteins and their random coil structure, suggests the major mechanism by which silk proteins cohere into fibers is the entanglement of disordered protein chains (Fig. 8). As such, the silk is more similar to protein materials formed from intrinsically unstructured proteins—such as the capture threads of velvet worms (phylum Onichophora; Haritos et al., 2010) and many bioadhesives (Graham 2008)—than to previously described silk fibers (Sutherland et al., 2010). Previously, ordered molecular structures in insect silk fibers have been viewed as a continuation of the liquid crystallinity of protein solutions within insect silk glands (Sutherland et al., 2010), which was in turn viewed as a necessary requirement to reduce the flow viscosity of protein solutions sufficiently to allow drawing through a spinneret (Kojic et al., 2006; Vollrath and Knight, 2001). We suggest such constraints are mitigated during fabrication of silverfish silk for two reasons. Firstly, the morphology of silverfish silk glands differs from that of spider silk glands, having a much smaller ratio between maximum and minimum diameters, and being much shorter in length (Bitsch, 1990). Both of these features are expected to reduce the drawing forces required to overcome flow viscosity (Kojic et al., 2006; Vollrath and Knight, 2001). Secondly, silverfish silk may be fabricated from more dilute protein solutions in comparison to other silks, similar to the fabrication of Onychophoran prey-capture threads from low-viscosity solutions containing only around 5% intrinsically disordered protein (Haritos et al., 2010). Fabrication from protein solutions at low concentration would also be expected to reduce shear forces during fabrication, allowing proteins to retain their solution structure. Overall, our results suggest the process of insect silk fabrication to be more flexible than previously appreciated, with the process of drawing through a spinneret determining the macroscopic form of the material as a cylindrical fiber, but imposing surprisingly few constraints at the level of molecular structure.

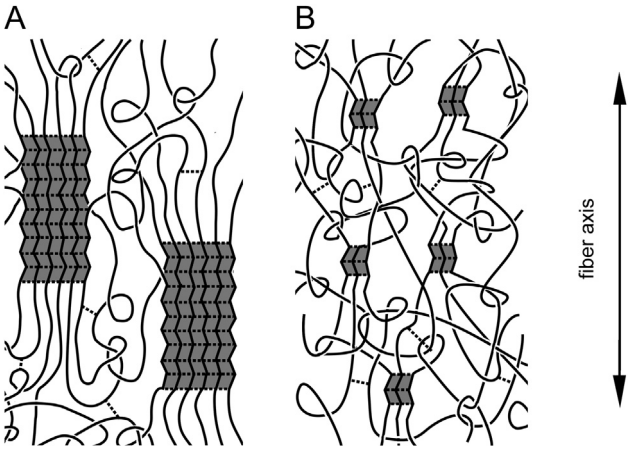

Fig. 8. Entanglement as the major form of cohesion in silverfish silk. A, classic conception of molecular organization in silk fibers made by silkworms and spiders, showing intermolecular H-bonding within beta-sheet crystallites and entanglement in disordered regions, after Termonia (1994). B, an equivalent cartoon for silverfish silk, a material in which the majority of protein is present as unordered (random coil) protein chains, with a lesser extended-beta-sheet (IIß) component.

Silks are semi-crystalline polymers in which a balance exists between ordered protein structures and disordered protein chains—each of which confer distinct mechanical and physical properties to the finished material (Krasnov et al., 2008). Ordered regions are associated with strength (Krasnov et al., 2008) and resistance to proteolysis (Arai et al., 2004), while disordered regions confer flexibility (Krasnov et al., 2008) and adhesiveness (Graham, 2008). An inference can be made regarding the relative importance of such properties in silverfish silk by invoking a comparison to other silks produced in insect epidermal glands. For example, silk fibers made by web-spinners (order Embioptera) are used to form protective galleries, and must remain structurally sound for long periods of time—up to weeks or months (Edgerly et al., 2002). Accordingly, web-spinner silk is predominantly composed of proteins with well-defined beta-sheet secondary structure (Collin et al., 2009; Okada et al., 2008). In contrast, silverfish silk is not required to bear any significant loads and needs to persist only for the duration of mating, approximately half an hour (Sturm, 1956); a predominantly random coil conformation may be well-suited to its required physical properties.

In addition to affecting the physical properties of solid fibers, the degree of structure within silk proteins has repercussions for which mechanisms of material fabrication are suitable. For silks that do not require a high content of ordered protein structures, entanglement may be an efficient method of fiber fabrication. If selection pressure for ordered structures in the solid fibers is weak, selection specifically for the open and extended random coil structure—which will promote maximal entanglement during fabrication, and is likely to increase the adhesiveness of the fibers—may dominate. The key defining feature of silverfish silk is the predominance of disordered protein chains. The other unusual features of the silk are likely consequences of the random coil molecular structure: the small residues Ala, Ser and Gly, which are associated with dense protein packing and ordered secondary structural elements in other silks, occur at relatively low frequency; the low proportion of protein in the orientated IIß component yields low birefringence; and randomly coiled protein chains are highly accessible to solvent, resulting in the low stability of the fibers in aqueous solvent.

In this study we have shown that the fabrication of silk fibers by entanglement of randomly coiled proteins is compatible with the physical constraints of fiber fabrication by drawing a protein solution through a spinneret. We have discussed how the function of a silk affects the balance between molecular order and disorder in silk fibers, and put forward silverfish silk as an example of a situation in which disorder is favored. Overall, this study suggests that in the broad sense, insect silks tend to contain well-defined protein secondary structures because of the mechanical and physical properties they confer to fibers. For fibers with less stringent material requirements, entanglement is an alternative mechanism of molecular cohesion that is capable of substituting for intermolecular bonding.

4. Materials and methods

4.1. Insects and silk collection

Domestic silverfish (*Ctenolepisma longicaudata*) were collected from human residences in Canberra (ACT, Australia) and housed in a glass tank heated to 25–30 °C, with pieces of black plastic card 'leaf-litter' for shelter. Bread crumbs, tropical fish flakes and water were provided for sustenance. Pieces of plastic card were removed periodically and examined for naturally spun silk, which could be collected with tweezers. Alternatively, males were cooled at −20 °C for 30 s and immobilized using sticky tape. Silk could be then drawn manually by brushing the phallic glands with a toothpick or pipette tip and winding the resulting fibers around a spindle.

4.2. Microscopy

Light microscopy was performed using a Leica M205C polarizing microscope (Leica, Wetzlar, Germany). Samples of naturally spun silk for electron microscopy were mounted on stubs using conductive tape, sputter-coated with gold and examined using a Zeiss Evo LS15 scanning electron microscope (Zeiss, Jena, Germany). Silk was visualized under high vacuum, using an accelerating voltage of 15 kV.

4.3. Solubilization and electrophoresis

Silk bundles manually drawn from the phallic glands of individual males were solubilized in 3% SDS, and the resulting solutions were used for polyacrylamide gel electrophoresis under reducing conditions using NuPage 4–12% Bis-Tris gels and 2-(N-morpholino) ethanesulfonic acid running buffer (Invitrogen, Carlsbad, CA, USA). Gels were stained with Coomassie Brilliant Blue (Sigma–Aldrich, St. Louis, MO, USA).

4.4. Raman and FTIR spectroscopy

Infrared spectra and Raman survey spectra were obtained from silk manually collected from males (as described in Section 4.1). These were bundles of parallel fibers of about 1 μm in diameter. For micro-Raman spectroscopy the fibers were aligned with the fiber axis parallel to the laser polarization using a rotating stage. The Raman spot size was of the order of 0.8 μm in diameter so one or two fibers could be included in the analysis volume. For infrared spectroscopy, the area analyzed was approximately 10 μm wide by 20 μm long. The maximum absorbance was less than 1 unit suggesting the sample analyzed could be 4 or 5 fibers thick. Polarized Raman spectra were obtained from naturally spun single fibers.

Wool fibers (18 μm diameter) from pen-fed Australian merino sheep were solvent scoured by gentle agitation in dichloromethane for 5 min. The solvent was decanted and the wool was compressed to remove as much solvent as possible. This process was performed three times. The above procedure was then repeated using ethanol and then deionized water, and then the wool was immersed in methanol, drained, and allowed to air dry. The lipids were then Soxhlet extracted from the wool by refluxing for 24 h with chloroform/methanol (70%/30% v/v). After extraction, the wool was dried in an oven at 107 °C. Muga cocoon silk was degummed using 2% sodium carbonate solution and 1% olive oil soap (based on weight of silk cocoon). The process was carried out at 98 °C for 2 h in a laboratory dying machine.

Raman spectra were obtained using an inVia confocal microscope system (Renishaw, Gloucestershire, UK) with 514 nm excitation from an argon ion laser through a ×50 (0.75 na) objective. Incident laser power was 4.86 mW as measured using a Nova power meter fitted with a PD300-3W head (Ophir Optronics Solutions Ltd., Israel). Survey spectra were collected over the range 3500 to 100 cm^{-1} and averaged over at least five scans, each with an accumulation time of 25 s. Polarization measurements were made in static mode covering the range 1800 to 1370 cm^{-1}. Fibers were orientated with respect to the laser polarization using a rotating stage. The laser polarization was rotated using a ½-wave plate while the spectrometer was fitted with a polarization analyzer consisting of a polarizer and a ½-wave plate. The polarized spectra were corrected to account for the polarization dependence of the optics of the Raman microscope using the factor determined from the ratio of the cross-polar spectra. The Raman shifts were calibrated using the 520 cm^{-1} line of a silicon wafer. The spectral resolution was ~1 cm^{-1}.

Infrared spectra were collected in transmission mode using a Perkin Elmer System 2000 FTIR spectrometer fitted with an i-series infrared microscope. Spectra were collected from 4500 to 750 cm^{-1} at 4 cm^{-1} resolution with 64 scans co-added. All data manipulation and deconvolution was carried out using Grams AI software version 9.1 (Thermo Fisher Scientific Inc., USA). Spectral deconvolution was carried out by first identifying band components from the second derivative spectra obtained using the Savitzky-Golay method (Savitzky and Golay, 1964). Fits are based on the usage of a minimal number of band components. All peaks heights were limited to the range greater than or equal to zero. In the initial fitting steps the band centers were only allowed to vary by ±5 cm^{-1} from the frequency determined by the second derivative spectra. In the final refinements all parameters were allowed to vary unconstrained. Two point linear baselines were used throughout.

4.5. Amino acid composition

To acquire a sufficient amount of silk for amino acid analysis, silk from the phallic glands of 19 males were wound around the same spindle and washed in milliQ water. Amino acid analysis was performed as a commercial service at the Australian Proteome Analysis Facility (Macquarie University, NSW, Australia). Samples underwent 24 h gas phase hydrolysis with 6 N HCl at 110 °C, and amino acids were analyzed using the Waters AccQTag Ultra chemistry. Cys and Trp residues were not analyzed by this method.,

Acknowledgments

The authors would like to thank Roger Jones, Holly Trueman and Shoko Okada for reviewing the manuscript, Dr. Rangam Rajkhowa of Deakin University for providing muga cocoon silk, and the many kind people who collected and donated silverfish. The authors are grateful for financial support for this project from Commonwealth Scientific and Industrial Research Organisation and an Australian National University PhD Scholarship. This research was facilitated using infrastructure provided by the Australian Government through the National Research Infrastructure Strategy (NCRIS), namely the Australian Proteomic Analysis Facility (APAF).

Appendix A. Supplementary data

Supplementary data related to this article can be found at http://dx.doi.org/10.1016/j.ibmb.2013.03.014.

References

Alberti, V.G., Storch, V., 1976. Ultrastructural investigations on the silk glands of Embioptera (Insecta). Zoologischer Anzeiger 197, 179–186. (S).

Arai, T., Freddi, G., Innocenti, R., Tsukada, M., 2004. Biodegradation of *Bombyx mori* silk fibroin fibers and films. Journal of Applied Polymer Science 91 (4), 2383–2390.
Ashton, N.N., Taggart, D.S., Stewart, R.J., 2012. Silk tape nanostructure and silk gland anatomy of trichoptera. Biopolymers 97 (6), 432–445.
Bitsch, J., 1990. Ultrastructure of the phallic glands of the firebrat, *Thermobia domestica* (Packard) (Thysanura: Lepismatidae). International Journal of Insect Morphology and Embryology 19 (2), 65–78.
Byler, D.M., Susi, H., 1986. Examination of the secondary structure of proteins by deconvolved FTIR spectra. Biopolymers 25 (3), 469–487.
Carter, E.A., Fredericks, P.M., Church, J.S., Denning, R.J., 1994. FT-Raman spectroscopy of wool. Spectrochimica Acta, Part A: Molecular and Biomolecular Spectroscopy 50A, 1927–1936.
Case, S.T., Cox, C., Bell, W.C., Hoffman, R.T., Martin, J., Hamilton, R., 1997. Extraordinary conservation of cysteines among homologous *Chironomus* silk proteins sp185 and sp220. Journal of Molecular Evolution 44 (4), 452–462.
Church, J.S., Corino, G., Woodhead, A.L., 1997. The Raman spectra of cortical and cuticle cells and some proteins isolated from wool. Biopolymers 42 (1), 7–17.
Collin, M.A., Garb, J.E., Edgerly, J.S., Hayashi, C.Y., 2009. Characterization of silk spun by the embiopteran, *Antipaluria urichi*. Insect Biochemistry and Molecular Biology 39, 75–82.
Edgerly, J.S., Davilla, J.A., Schoenfeld, N., 2002. Silk spinning behavior and domicile construction in webspinners. Journal of Insect Behavior 15 (2), 219–242.
Fabian, H., Anzenbacher, P., 1993. New developments in Raman spectroscopy of biological systems. In: Durig, J.R. (Ed.), Vibrational Spectroscopy. Elsevier Science, Amsterdam, pp. 125–148.
Frushour, B.G., Koenig, J.L., 1975. Raman spectroscopy of proteins. In: Clark, R.S.H., Hester, R.E. (Eds.), Advances in Infrared and Raman Spectroscopy. Heyden, New York, pp. 35–97.
Fu, C., Shao, Z., Vollrath, F., 2009. Animal silks: their structures, properties and artificial production. Chemical Communications, 6515–6529.
Graham, L.D., 2008. Biological adhesives from nature. In: Bowlin, G., Wnek, G. (Eds.), Encyclopedia of Biomaterials and Bioengineering. Informa Healthcare, New York, pp. 236–253.
Haritos, V.S., Niranjane, A., Weisman, S., Trueman, H.E., Sriskantha, A., Sutherland, T.D., 2010. Harnessing disorder: onychophorans use highly unstructured proteins, not silks, for prey capture. Proceedings of the Royal Society B: Biological Sciences 277 (1698), 3255–3263.
Hepburn, H.R., Chandler, H.D., Davidoff, M.R., 1979. Extensometric properties of insect fibroins: the green lacewing cross-beta, honeybee alpha-helical and greater waxmoth parallel-beta conformations. Insect Biochemistry 9 (1), 69–77.
Kojic, N., Bico, J., Clasen, C., McKinley, G.H., 2006. *Ex vivo* rheology of spider silk. Journal of Experimental Biology 209 (21), 4355–4362.
Krasnov, I., Diddens, I., Hauptmann, N., Helms, G., Ogurreck, M., Seydel, T., Funari, S.S., Müller, M., 2008. Mechanical properties of silk: Interplay of deformation on macroscopic and molecular length scales. Physical Review Letters 100 (4).
Lefèvre, T., Paquet-Mercier, F., Rioux-Dubé, J.-F., Pézolet, M., 2012. Structure of silk by Raman spectromicroscopy: from the spinning glands to the fibers. Biopolymers 97 (6), 322–336.
Lucas, F., Rudall, K.M., 1968. Variety in composition and structure of silk fibroins: some new types of silk from the Hymenoptera. In: Crewther, W.G. (Ed.), Symposium on Fibrous Proteins. Butterworths, Australia.
Maiti, N.C., Apetri, M.M., Zagorski, M.G., Carey, P.R., Anderson, V.E., 2004. Raman spectroscopic characterization of secondary structure in natively unfolded proteins: α-synuclein. Journal of the American Chemical Society 126 (8), 2399–2408.
Nagashima, T., Niwa, N., Okajima, S., Nonaka, T., 1991. Ultrastructure of silk gland of webspinners, *Oligotoma japonica* (Insecta: Embioptera). Cytologia 56, 679–685.
Nogami, N., Sugeta, H., Miyazawa, T., 1975. C–S Stretching vibrations and molecular conformations of isobutyl methyl sulfide and related alkyl sulfides. Bulletin of the Chemical Society of Japan 48 (9), 2417–2420.
Okada, S., Weisman, S., Trueman, H.E., Mudie, S.T., Haritos, V.S., Sutherland, T.D., 2008. An Australian webspinner species makes the finest known insect silk fibers. International Journal of Biological Macromolecules 43 (3), 271–275.
Porter, D., Vollrath, F., 2009. Silk as a biomimetic ideal for structural polymers. Advanced Materials 21, 487–492.
Roessingh, P., 1989. The trail following behaviour of *Yponomeuta cagnagellus*. Entomologia Experimentalis et Applicata 51 (1), 49–57.
Rousseau, M.-E., Lefèvre, T., Beaulieu, L., Asakura, T., Pézolet, M., 2004. Study of protein conformation and orientation in silkworm and spider silk fibers using Raman microscopy. Biomacromolecules 5, 2247–2257.
Rudall, K.M., 1962. Silk and other cocoon proteins. In: Florkin, M., Mason, H.S. (Eds.), Comparative Biochemistry. Academic Press, New York, pp. 397–433.
Savitzky, A., Golay, M.J.E., 1964. Smoothing and differentiation of data by simplified least squares procedures. Analytical Chemistry 36 (8), 1627–1639.
Serrao, J.E., 2005. Ultrastructure of the silk glands in three adult females of sphecid wasps of the genus *Microstigmus* (Hymenoptera: Pemphredoninae). Revista Chilena de Historia Natural 78, 15–21.
Shultz, J.W., Regier, J.C., 2000. Phylogenetic analysis of arthropods using two nuclear protein-encoding genes supports a crustacean + hexapod clade. Proceedings of the Royal Society B: Biological Sciences 267 (1447), 1011–1019.
Siamwiza, M.N., Lord, R.C., Chen, M.C., Takamatsu, T., Harada, I., Matsuura, H., Shimanouchi, T., 1975. Interpretation of the doublet at 850 and 830 cm^{-1} in the Raman spectra of tyrosyl residues in proteins and certain model compounds. Biochemistry 14 (22), 4870–4876.
Singh, B.R., DeOliveira, D.B., Fu, F.-N., Fuller, M.P., 1993. Fourier transform infrared analysis of amide III bands of proteins for the secondary structure estimation. In: Nafie, L.A., Mantsch, H.H. (Eds.). SPIE, Los Angeles, CA, USA, pp. 47–55.
Sturm, H., 1956. Die paarung beim silberfischchen, *Lepisma saccharina*. Zeitschrift fur Tierpsychologie 13, 1–12.
Sturm, H., 1987. The mating behaviour of *Thermobia domestica* (Packard) (Lepismatidae, Zygentoma, Insecta). Braunschweiger Naturkindliche Schriften 2 (4), 693–711.
Sturm, H., 1997. The mating behaviour of *Tricholepidion gertschi* Wygod., 1961 (Lepidotrichidae, Zygentoma) and its comparison with the behavioiur of other Apterygota. Pedobiologa 41, 44–49.
Sturm, H., Machida, R., 2001. Archaeognatha. Walter de Gruyter, New York.
Sugeta, H., Go, A., Miyazawa, T., 1972. S-S and C-S stretching vibrations and molecular conformations of dialkyl disulfides and cystiene. Chemistry Letters, 83–86.
Sutherland, T.D., Campbell, P.M., Weisman, S., Trueman, H.E., Sriskantha, A., Wanjura, W.J., Haritos, V.S., 2006. A highly divergent gene cluster in honey bees encodes a novel silk family. Genome Research 16 (11), 1414–1421.
Sutherland, T.D., Young, J.H., Weisman, S., Hayashi, C.Y., Merritt, D.J., 2010. Insect silk: one name, many materials. Annual Review of Entomology 55, 171–188.
Sutherland, T.D., Weisman, S., Walker, A.A., Mudie, S.T., 2011. The coiled coil silk of bees, ants and hornets. Biopolymers 97 (6), 446–454.
Termonia, Y., 1994. Molecular modelling of spider silk elasticity. Macromolecules 27, 7378–7381.
Van Wart, H.E., Scheraga, H.A., 1986. Agreement with the disulfide stretching frequency-conformation correlation of Sugeta, Go, and Miyazawa. Proceedings of the National Academy of Sciences of the United States of America 83, 3064–3067.
Vollrath, F., Knight, D.P., 2001. Liquid crystalline spinning of spider silk. Nature 410 (6828), 541–548.
Watson, J.A.L., Li, C.S., 1967. A further pest species of silverfish (Thysanura) from Australia, with a key to the domestic species. Journal of the Australian Entomological Society 6, 89–90.
Weisman, S., Okada, S., Mudie, S.T., Huson, M.G., Trueman, H.E., Sriskantha, A., Haritos, V.S., Sutherland, T.D., 2009. Fifty years later: the sequence, structure and function of lacewing cross-beta silk. Journal of Structural Biology 168 (3), 467–475.